Time-frequency analysis of laser speckle contrast for transcranial assessment of cerebral blood flow

Nadezhda Golubova[a,1], Elena Potapova[a,1], Evgeniya Seryogina[a], Viktor Dremin[a,b,*]

[a] *Research and Development Center of Biomedical Photonics, Orel State University, Orel, Russia*
[b] *College of Engineering and Physical Sciences, Aston University, Birmingham, UK*

Abstract

Improving noninvasive approaches to monitoring blood microcirculation is an urgent topic in modern biomedical engineering. One of the actively developing methods is laser speckle contrast imaging (LSCI), which allows not only the visualization of microvessels but also the quantitative measurements of microcirculatory blood flow. This work shows the application of LSCI for mapping the cerebral vessels of a laboratory animal, and also presents the time-frequency processing of the registered signal. Thus, we expand the capabilities of the existing LSCI approach and demonstrate spatial mapping of blood flow rhythms. The proposed technology makes it possible not only to measure the relative cerebral blood flow but also to expand diagnostic capabilities for a detailed analysis of the physiological mechanisms of changes in blood flow.

Keywords: laser speckle contrast imaging, cerebral blood flow dynamics, wavelet transform

1. Introduction

The proper functioning of the blood microcirculation system is of great importance, as it provides the delivery of nutrients and oxygen to biological tissues and evacuates toxins and waste products. There is increasing evidence that microcirculatory system dysfunction plays an important role

*Corresponding author: viktor.dremin@bmecenter.ru
[1]These authors contributed equally to this work.

in the pathogenesis of various brain diseases [1, 2]. As a result, cerebral microcirculation appears to be a therapeutic target in treatment.

Cerebral blood flow is largely adjusted by the mechanism of cerebral autoregulation, which protects brain tissue from a decrease in blood perfusion [3]. In turn, autoregulation of cerebral blood flow functions occurs through myogenic, metabolic, and neurogenic mechanisms [4]. Therefore, by analyzing these mechanisms, it is possible to obtain valuable diagnostic information on the state of cerebral blood flow [5]. Over the years of studying oscillatory processes in the human microcirculation system, researchers described the clinical and physiological aspects of cardiac, breath-dependent, myogenic, neurogenic, and endothelial blood flow oscillations [6, 7, 8].

Nowadays, laser Doppler flowmetry (LDF) has become a well-established and widely used technology to monitor blood microcirculation. This method is also actively used to assess cerebral blood flow [9, 10, 11, 12]. However, it has limitations such as potential large variations in the obtained results depending on the detector placement due to single-point implementation of measurements. It is worth noting that imaging technology with spatio-temporal resolution that utilizes the laser Doppler effect also exists. Laser Doppler imaging (LDI) is a technique that uses a laser beam to scan biological tissues. Although LDI shows great potential for clinical applications [13], including the study of cerebral blood flow [14, 15], it is quite challenging to implement and requires additional time to collect and process data.

Recently, laser speckle contrast imaging (LSCI) has been widely used to image blood flow in biological tissues. The ability to map blood flow makes the technique applicable in the studies of blood microcirculation in various medical and scientific cases [16, 17, 18, 19, 20]. LSCI technology has been extensively applied to visualize regional cerebral blood flow [21, 22, 23, 24, 25, 26, 27].

To monitor blood flow using the LSCI method, clinicians have a dataset that contains multiple images (perfusion maps) representing the temporal evolution of blood flow in the study area. This provides the possibility of performing a frequency analysis of the acquired signal in areas of interest [28, 29, 30, 31, 32, 33, 34]. The analysis of blood oscillations in the LSCI technique seems promising, since the method is simple to implement and provides visualization of the entire area of investigation with high spatial and temporal resolution [35]. Thus, LSCI has clear advantages over LDF and LDI. Using LSCI, it is possible to obtain a blood circulation map and identify areas with microvessels for further signal processing. Recent studies confirm

that the temporal variations of the blood flow oscillations measured by LSCI correlate well with the oscillations obtained by the LDF method [32]. This makes it possible to use the same frequency analysis methods for LSCI that have been used for LDF for a long time.

In this paper, we present the results of time-frequency analysis of laser speckle contrast recording transcranially on the laboratory rat brain, produced using a new method of LSCI data processing and representation. We also present the results of preliminary studies on a phantom simulating the oscillatory motion of a liquid through a glass capillary.

2. Materials and Methods

2.1. Experimental Setup

Experimental studies were carried out using a specially developed experimental setup shown in Fig. 1. The investigated area was illuminated with the LDM785 laser source (Thorlabs, USA) with a light power of 20 mW and a wavelength of 785 nm through the set of diffusers (Thorlabs, USA). The backscattered light was collected via a high-resolution UI-3360CP-NIR-GL CMOS camera (IDS, USA). To eliminate single scattering, a NIR linear polarizer (Thorlabs, USA) was placed in front of the MVL25TM23 camera objective (Thorlabs, USA). The images were obtained for 90 FPS and 11 ms exposure time for all experiments.

2.2. Data Processing

Two different processing pipelines were used for the analysis of different regions of interest (ROIs) and the full (pixel-wise) image analysis. This is summarized in Fig. 2, and explained below.

Raw speckle images were processed using an original algorithm developed in Matlab R2019b software. Depending on the selected parameters, the algorithm allows one to process spatial, temporal, or spatio-temporal speckle contrast [16]. Accordingly, using the temporal or spatial standard deviation of the speckle intensity, the average speckle contrast can be calculated as follows:

$$K = \frac{\sigma}{\langle I \rangle}, \tag{1}$$

where $\langle I \rangle$ is the mean intensity value and σ is the intensity standard deviation.

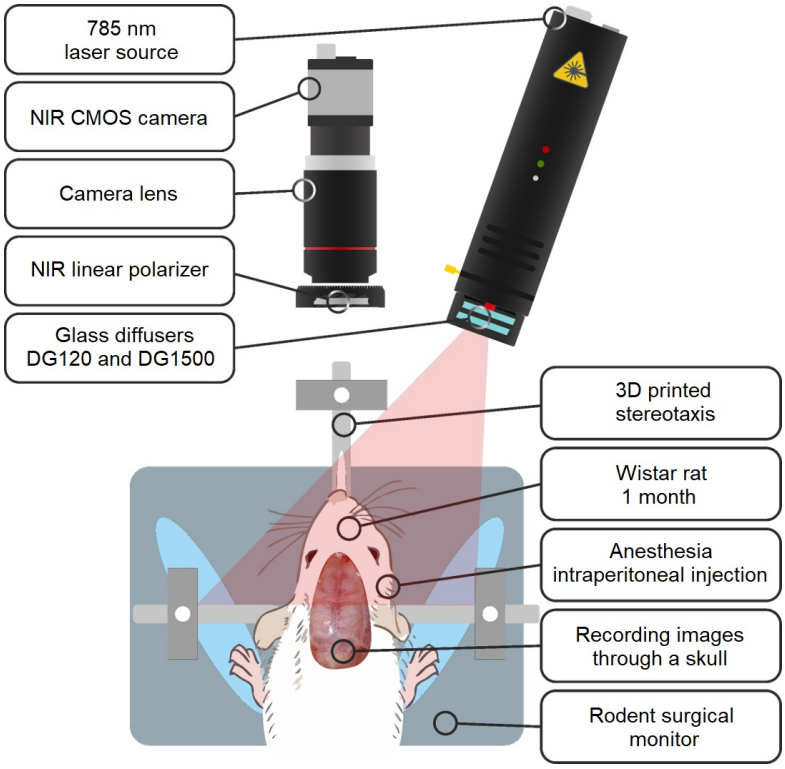

Figure 1: Scheme of the developed LSCI experimental setup and auxiliary equipment.

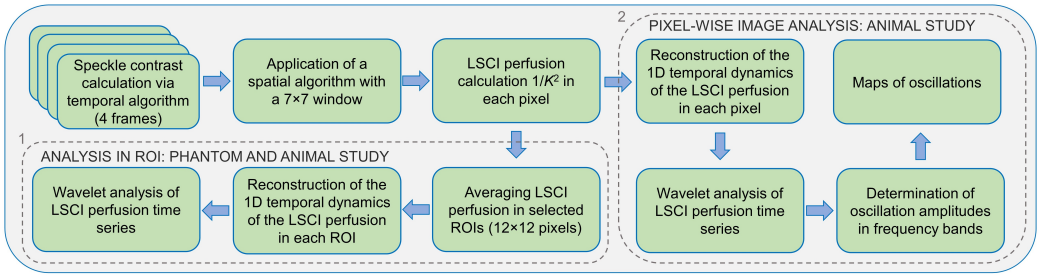

Figure 2: Flowchart of LSCI data processing explaining the steps of the analysis algorithm of the selected ROIs (1) and the full image (2).

If moving scattering particles are present in the object illuminated by coherent light, then the blurring of the speckle image recorded by the camera will result in the observed standard deviation of the intensity being lower than for a completely static set of scatterers, and therefore the speckle image

contrast will also be reduced. The average velocity of the scattering particles is inversely proportional to the characteristic correlation time of the intensity of the observed speckle dynamics, τ_c [36]. The described behavior of the speckle contrast value can be quantitatively analyzed as follows [37, 38]:

$$K = \frac{\sigma}{\langle I \rangle} = \left\{ \beta \left\{ \frac{\tau_c}{T} + \frac{{\tau_c}^2}{2T^2} \left[\exp\left(\frac{-2T}{\tau_c} \right) - 1 \right] \right\} \right\}^{1/2}, \tag{2}$$

where β is a constant depending on the parameters of the optical system and T is the exposure time.

To visualize the brain vessels in a better quality, raw speckle images were processed with a number of frames for a temporal averaging equal to 90. Thus, the data was averaged over one second of recording. After temporal averaging, we additionally applied a spatial algorithm with a window equal to 7. For frequency analysis, we used time averaging over 4 frames and spatial averaging with the same window. Therefore, the initial frame rate (90 FPS) was reduced to 22.5 FPS. The search for optimal parameters was especially important because it was necessary to maintain a sufficient sampling rate of the signal for reliable frequency analysis.

According to studies on the equivalence and differences between LDF and laser speckle contrast analysis, to perform the same frequency decomposition method as in LDF, the LSCI perfusion values were calculated as $1/K^2$ [39, 40].

The time-frequency analysis of the obtained perfusion value was performed by the continuous wavelet transform (CWT). Perfusion signals were decomposed using CWT in the form [41]:

$$W_x(s,\tau) = \frac{1}{\sqrt{s}} \int_{-\infty}^{\infty} x(t) \psi^* \left(\frac{t-\tau}{s} \right) dt, \tag{3}$$

where $x(t)$ is a target signal, τ is the time shift of the wavelet, s is the scaling factor, and the symbol * means complex conjugation. The decomposition was performed using the Morlet wavelet [42]:

$$\psi(t) = e^{2\pi i t} e^{-t^2/2\sigma^2}. \tag{4}$$

The Morlet wavelet is one of the most commonly used wavelets. This is the most reliable wavelet for timefrequency analysis of non-stationary time series data, in particular of biological nature. The resulting spectrum con-

tained 9 octaves that made it possible to observe all five frequency ranges of blood microcirculation regulation found in animals [43, 44].

2.3. Phantom Experiments

The phantom experiments aimed to test the system's ability to identify the difference between various solution velocities and also to register solution flow oscillations. As a phantom, a capillary tube with an internal diameter of 1.6 mm and an electric pump calibrated according to the velocity of the liquid were used. The detailed description and general appearance of the phantom are shown in one of our previous work [17]. An 8% solution by volume of Intralipid 20% (Fresenius Kaby, USA) was pumped through the capillary using an electric pump. The selected 8% Intralipid concentration approximately corresponds to the optical scattering properties of blood at a wavelength of 785 nm (μ_s = 72 mm^{-1}) [45, 46]. The Intralipid solution was pumped through a capillary tube with linear velocities of 1 and 2 mm/s to cover the *in vivo* range of blood velocities.

In phantom experiments were obtained two-minute recordings for each velocity of liquid flow in the capillary. The processing of the data was carried out according to the algorithm described in Section 2.2 and resulted in laser speckle contrast images with a resolution of 500×500 pixels. A 12×12 pixels ROI in the central part of the tube was selected and the value of the spatio-temporal speckle contrast K was calculated using Eq. 1.

2.4. Animal Study

In the animal part of the study, a one-month-old Wistar rat (male) with an initial body weight of 100 g was used. The experimental studies were carried out in accordance with the principles of GLP. The work was approved by the Ethics Committee of Orel State University (protocol No.12 dated 6 September 2018). The study protocol included animal anesthesia by intramuscular injection of Zoletil/Xyla drug composition in standard proportions and dosages. The animals were placed on a heated table (37 °C) to maintain stable body temperature. After that, the animal was fixed in a 3D printed stereotaxis to avoid movement artifacts. To access the study area (cerebral), the skin was cut and removed from the head of the animal. The animal's skull was not removed and therefore a noninvasive transcranial cerebral imaging was performed [47, 48, 49, 27, 24]. During the *in vivo* experiments, the surgical warming and monitoring system (model: Rodent Surgical Monitor+, Indus Instruments, USA) was used to monitor the physiological state of the

animal. It provides information such as multi-lead ECGs, heart rate values with the range from 200 to 999 beats per minute (BPM), respiration rate values with the range from 15 to 400 breaths per minute (BrPM), and core body temperature values up to 50 °C. The use of this system also made it possible to verify the information about cardiac and respiratory oscillations obtained by LSCI perfusion post-processing.

Speckle images were captured transcranially for 5 minutes. To study the dynamics of cerebral blood flow in various parts of the brain, three target areas were selected: the superior sagittal sinus, its tributaries, and brain areas that have no clearly visualized vessels. In each of the target areas, five ROI (12×12 pixels) were selected to obtain statistics (see Fig. 5). In addition, pixel-by-pixel wavelet analysis was used for a detailed study of the spatial frequency distribution, which made it possible to plot the oscillation maps.

3. Results

3.1. Phantom Experiments

The results of the laser speckle contrast imaging of capillaries with different solution flow velocities (1 and 2 mm/s) are shown in Fig. 3.

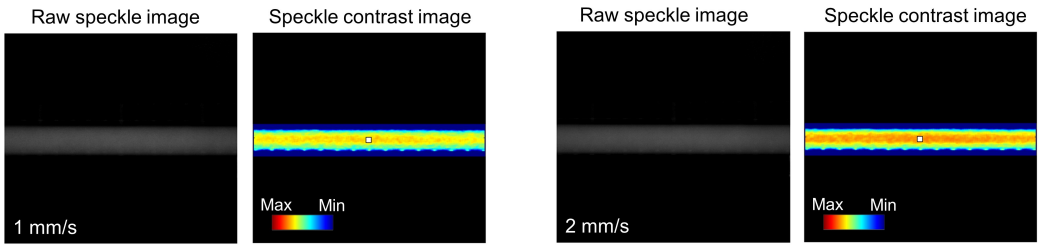

Figure 3: Raw and speckle contrast images of fluid motion in a capillary at different flow rates. The white square is the ROI analyzed.

The calculated contrast was transformed into pseudo-colors, where the high velocity of the scattering particle flow corresponded to red, and the low velocity corresponded to blue. This experiment shows that the built-in setup is capable of detecting changes in the flow rate of scattering particles.

The results of the CWT analysis for the capillary phantom are shown in Fig. 4. First, the obtaining of the LSCI signal for each of two velocity variations was performed in accordance with formula $1/K^2$. Then, the wavelet

transform was used, which made it possible to obtain amplitude scalograms and averaged wavelet spectra for different flow rates.

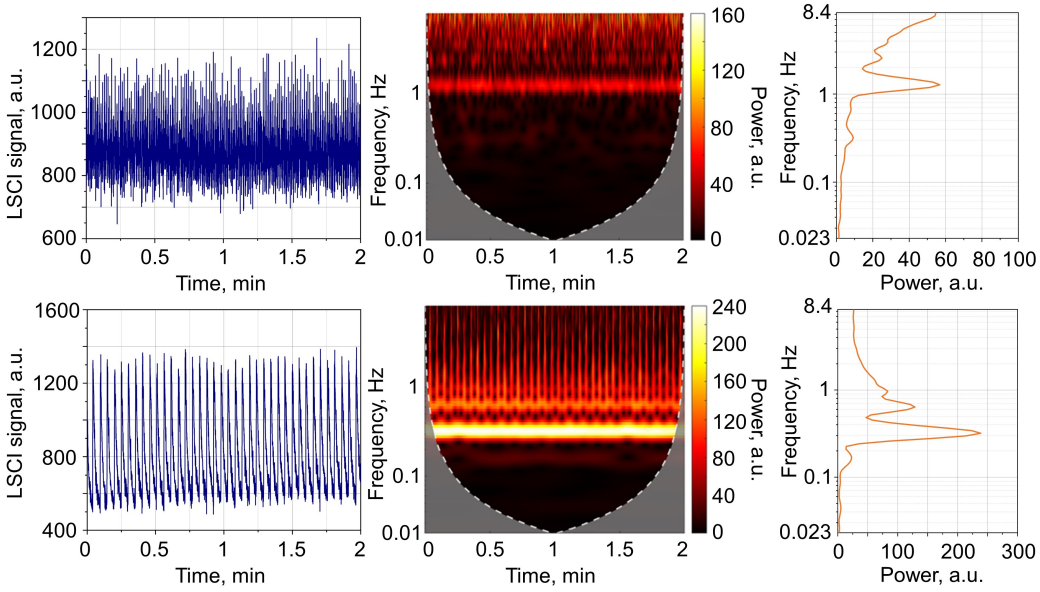

Figure 4: Wavelet analysis of laser speckle contrast signals obtained for the capillary phantom. First row: laser speckle contrast signal from the selected ROI, CWT amplitude scalogram, and time-averaged wavelet spectrum for 1 mm/s flow velocity; second row shows the same types of data for 2 mm/s flow velocity. The white dashed line and the shaded area show the cone of influence where edge effects become significant at different frequencies.

The obtained results show that for various solution flow velocities, there are different frequency distributions. For 1 mm/s and 2 mm/s, there are multiple peaks in the wavelet spectra, indicating that the needed rate of administration is achieved by pulsations of several frequencies. At a given Intralipid flow rate of 1 mm/s in the capillary, oscillations at a frequency of approximately 1.28 Hz were detected. At a higher fluid flow rate (2 mm/s), high-frequency oscillations of 0.64 Hz were modulated by a low frequency of about 0.32 Hz.

3.2. Animal Study

The next step was to conduct studies of dynamic changes in the cerebral blood circulation of the rat. Fig. 5 shows images of the rat brain obtained on the camera in initial monochrome mode, as well as the speckle contrast image.

For wavelet decomposition, zones with very different blood flow dynamics were selected: the superior sagittal sinus, its tributaries, and brain areas that do not have clearly visualized vessels. Areas with higher blood flow, such as large vessels, have lower speckle contrast values and appear yellow in the images.

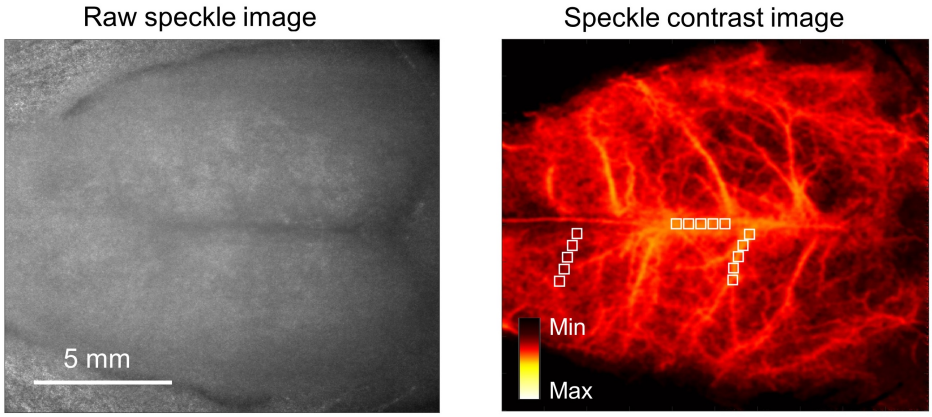

Figure 5: Raw speckle and processed images of the rat brain obtained transcranially. The white squares indicate ROIs for wavelet analysis.

Fig. 6 shows the results of the wavelet analysis of the obtained perfusion in each target area.

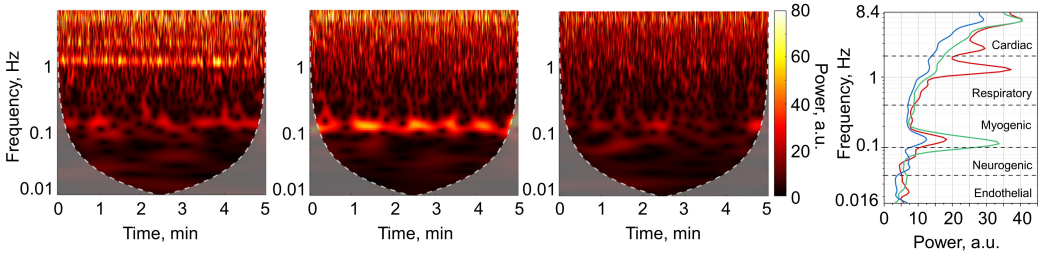

Figure 6: Wavelet analysis of obtained perfusion values: (a) example of CWT amplitude scalogram for the superior sagittal sinus (red line in d), (b) tributary (green line in d), and (c) brain tissue that does not have clearly visualized vessels (blue line in d); (d) corresponding time-averaged spectra.

In the data for all target areas, there were prominent amplitudes of oscillations caused by vasomotions (0.11-0.13 Hz), respiratory activity (1.3 Hz), and heart beats (6.3-6.7 Hz). Vasomotion amplitude values vary from 12.5

to 33.7 a.u.; respiratory - from 13.3 to 37.2 a.u.; cardiac - from 29.2 to 40.6 a.u. (depending greatly on the target area that is analyzed). According to the data obtained from the monitoring system, the animal had 386 BPM (approximately 6.44 Hz) and 73 BrPM (approximately 1.22 Hz) on average. Fig. 6 also illustrates the fact that LSCI is sensitive to blood flow not only in visible superficial vessels, but also in tissue regions with vessels that are non-visible in the given speckle-contrast image. The presence of oscillations in such regions suggests that the dynamic characteristics of the speckle contrast contain information on the blood flow of the underlying microvessels.

Fig. 7 presents mean time-averaged spectra and standard deviations for five ROIs in each of the three target areas (see Fig. 5). This was done in order to acquire statistics on whether the wavelet spectrum shape repeats at different ROIs in the same region.

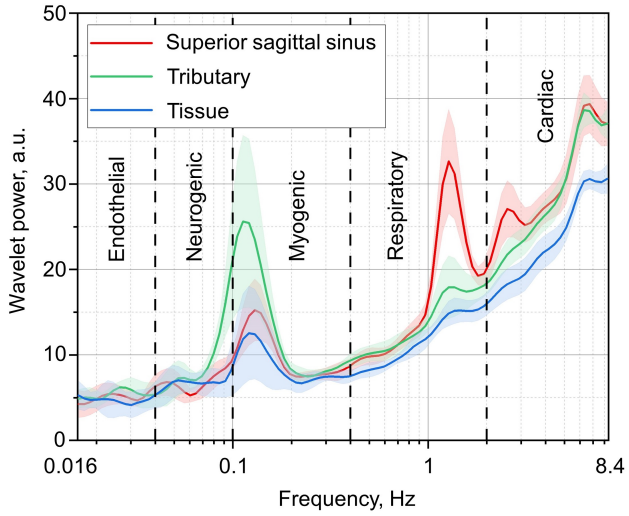

Figure 7: Mean time-averaged spectra (solid lines) and standard deviations (semi-transparent areas) for five ROIs in each of three target areas.

Based on the results of the calculation, the lowest scatter of values was found in the area without clearly visualized vessels for the cardiac oscillations. On the contrary, the tributary appeared as the region with the largest difference in values found for the myogenic oscillations.

Next, we performed a pixel-by-pixel wavelet analysis of perfusion and obtained oscillation distribution maps for the three dominant components (Fig. 8). A high amplitude of cardiac oscillations is observed fairly evenly in

large vessels over the entire surface of the rat brain. As expected, according to the mean time-averaged spectra calculated above, respiratory oscillations have a pronounced amplitude only in the central vessel, and myogenic oscillations are most pronounced in peripheral vessels of small diameter.

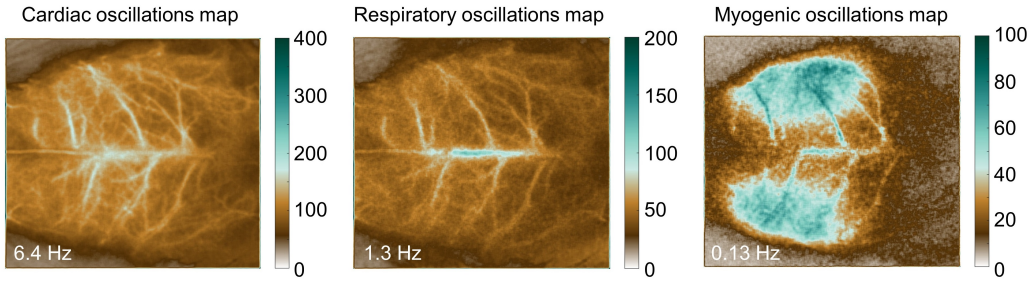

Figure 8: Spatial variations in cardiac (6.4 Hz), respiratory (1.3 Hz), and myogenic (0.13 Hz) activity.

It is worth noting that the calculation of the average wavelet spectrum is similar to the use of a time algorithm for calculating speckle contrast, which allows for high-quality visualization of the vascular network.

4. Discussion

The study of cerebral blood flow is an ideal application for laser speckle contrast imaging, given that blood vessels are very close to the surface, so it allows recording images with high signal-to-noise ratio in laboratory animals even without skull destruction. According to some authors [50], the diagnostic volume depth of the LSCI technology is 300 μm while using a laser source with a wavelength of about 780 nm. Analysis of perfusion map sequences recorded by the LSCI method in a simple hardware implementation has been shown to provide insight into perfusion dynamics in spatial and temporal dimensions.

The phantom of fluid motion with specified pulsations proposed by us allowed to experimentally investigate the reliability of time-frequency analysis of the laser speckle contrast method. Speckle data analysis was performed for two velocities of pulsating flow of the scattering fluid in the capillary tube. The velocities corresponded to the physiological parameters of blood flow in the cerebral capillaries and arterioles [51]. When analyzing the obtained speckle contrast images of fluid motion (Fig. 3), it can be concluded that the

proposed experimental system for the registration of speckle images provides visual indication of flow changes in the capillary when simulating different flow rates in it. Wavelet analysis of signals in the ROI (the central part of the fluid flow in the capillary) revealed pulsations caused by operating patterns of the perfusion plunger system (Fig. 4). The infusion rate in infusomats is not a constant parameter and has pulsations permitted by the manufacturer.

To assess the oscillations of cerebral blood flow *in vivo*, we used laser speckle imaging to monitor the relative changes in blood flow in the cerebral vascular system. Additionally, we used wavelet analysis to identify features of rhythmic activity. We provided continuous simultaneous monitoring of cardiac activity and respiratory rate to ensure that the cardiac and respiratory frequency ranges were correctly determined.

Vasomotions are of great interest since they are assumed to be related to local regulation of blood flow and can be used in various clinical and fundamental medical applications. The range of vasomotor activity can be further divided into shorter intervals depending on the vasomotor origin. T. Mastantuono et al. reported earlier that in the rat brain, oscillatory patterns characterize pial blood flow and the pial circulation of rats is regulated by the same mechanisms as the microcirculation of the human skin [52].

We found (Fig. 7) that cardiac oscillations (6.3–6.7 Hz) are present in the spectra of all ROIs and have a rather high amplitude even in tissue where vessels are not clearly visualized. Respiratory oscillations are most clearly observed in the central vessel, whereas the appearance of a peak that has a frequency twice higher than the respiratory rate requires additional study and explanation. At this point of investigation, we assume that the appearance of the peak may be due to physiological movement of bones and tissues. During the periodic cycle, the speckle structure depends on many variations that cause secondary frequencies other than the main frequency, including those associated with the movement of the skull bones and cerebral tissue during breathing. These secondary frequencies can lead to some misidentification of the real oscillation frequency and manifest as the second harmonic of the main frequency [53].

Cardiac and respiratory regulation is common to the entire microcirculatory system of the body, including the vascular system of the brain, therefore, as expected, we found these oscillations in all the studied ROIs. In the range of myogenic oscillations, repeatability of the peaks was also observed. In contrast to the ranges mentioned above, the oscillation spectra of the neurogenic and endothelial origins did not repeat each other in shape, suggesting

the spatial heterogeneity of these oscillations.

An interesting observation was the registered high intensity of myogenic oscillations in the peripheral vessel of the brain. Experimental works show that there is a longitudinal gradient of myogenic reactivity in the arteriolar system [54]. At the same time, relative myogenic reactivity increases with decreasing vessel diameter, which is most likely what we have seen in our work. However, the physiological significance of the myogenic range in the regulation of cerebral blood circulation is still under discussion [3, 52]. The origin of such signals in cerebral microcirculation is not definitively clear, and separating the effect of blood pressure fluctuations from vasomotor dynamics on cerebral hemodynamics is an unresolved problem [55].

The obtained oscillation maps in three frequency ranges (Fig. 8) allowed us to confirm that cardiac oscillations are manifested in almost all vessels, both large and peripheral. It also seems that the assumption of a stronger severity of myogenic oscillations in small-diameter vessels is confirmed by a map of myogenic oscillations, where higher values of amplitudes are observed at the periphery.

The visualization of rhythms proposed in the article based on the processing of speckle contrast images can play a great role both in fundamental medicine to clarify physiological mechanisms and in clinical practice to develop new diagnostic parameters. From our point of view, the proposed approach is most interesting to develop in the field of hemodynamics of both cerebral circulation and blood flow of other organs using functional tests (physiologically active substances, temperature tests, phototherapy, etc.).

5. Conclusions and Limitations

LSCI has become widely used in the last decade as it allows a quantitative assessment of changes in blood flow with high spatial and temporal resolution. In this paper we presented the results of time-frequency analysis of laser speckle contrast recording on the laboratory rat brain. The proposed technology makes it possible not only to measure the relative cerebral blood flow of the cerebral cortex, but also to expand diagnostic capabilities for detailed analysis of the physiological mechanisms of changes in cerebral blood flow. The developed approach can be useful for studying changes in cerebral blood flow, as well as peripheral blood flow in other areas, in a number of different applications, including the study of the effect of physiologically active substances or physical factors (e.g., laser radiation) on vascular blood

flow mechanisms.

In this paper, we do not analyze neurogenic and endothelial oscillations in detail. This is due to the relatively short perfusion records. This may be the subject of further research.

The proposed method is relatively easy to use, however, LSCI measures only relative blood flow, while absolute velocity values cannot be quantified at this stage of the setup realization. This could also be the subject of research improvement. Another limitation of the experiment is that blood flow monitoring using the LSCI method can be performed transcranially only in rats no older than one month. For adult rats, craniotomy may be required to obtain an accurate signal of cortical blood flow. An additional increase in penetration depth can be achieved using optical clearing methods [56].

Although the performance of the speckle contrast calculation algorithm allows real-time processing, the wavelet analysis for each pixel creates a bottleneck in the pipeline of the measurement procedure, thus imposing the main limitation on the method performance: large size of files created during processing, and as a result - a high amount of RAM needed. The use of powerful multi-core computing systems can significantly increase the speed of calculations. In addition, combining the presented spectral decomposition with machine learning methods [57] can further improve the analysis of speckle images.

Acknowledgements

The study was supported by the Russian Science Foundation under the project No. 22-75-10088.

References

[1] S. E. Erdener, T. Dalkara, Small vessels are a big problem in neurodegeneration and neuroprotection, Front. Neurol. 10 (2019) 889.

[2] Y. Kolinko, K. Krakorova, J. Cendelin, Z. Tonar, M. Kralickova, Microcirculation of the brain: morphological assessment in degenerative diseases and restoration processes, Rev. Neurosci. 26 (1) (2015) 75–93.

[3] S. Becker, F. Klein, K. Knig, C. Mathys, T. Liman, K. Witt, Assessment of dynamic cerebral autoregulation in near-infrared spectroscopy using

short channels: A feasibility study in acute ischemic stroke patients, Front. Neurol. 13 (2022).

[4] M. Reinhard, E. Wehrle-Wieland, D. Grabiak, M. Roth, B. Guschlbauer, J. Timmer, C. Weiller, A. Hetzel, Oscillatory cerebral hemodynamics – the macro- vs. microvascular level, J. Neurol. Sci. 250 (2006) 103–109.

[5] J. Myburgh, Quantifying cerebral autoregulation in health and disease, Crit. Care Resusc. 6 (2004) 59–67.

[6] A. Stefanovska, M. Bracic, H. Kvernmo, Wavelet analysis of oscillations in the peripheral blood circulation measured by laser doppler technique, IEEE. Trans. Biomed. Eng. 46 (10) (1999) 1230–1239.

[7] A. V. Dunaev, V. V. Sidorov, A. I. Krupatkin, I. E. Rafailov, S. G. Palmer, N. A. Stewart, S. G. Sokolovski, E. U. Rafailov, Investigating tissue respiration and skin microhaemocirculation under adaptive changes and the synchronization of blood flow and oxygen saturation rhythms, Physiol. Meas. 35 (4) (2014) 607.

[8] V. Dremin, I. Kozlov, M. Volkov, N. Margaryants, A. Potemkin, E. Zherebtsov, A. Dunaev, I. Gurov, Dynamic evaluation of blood flow microcirculation by combined use of the laser Doppler flowmetry and high-speed videocapillaroscopy methods, J. Biophotonics 12 (6) (2019) e201800317.

[9] J. Tonnesen, A. Pryds, E. H. Larsen, O. B. Paulson, J. Hauerberg, G. M. Knudsen, Laser Doppler flowmetry is valid for measurement of cerebral blood flow autoregulation lower limit in rats, Exp. Physiol. 90 (3) (2005) 349–355.

[10] B. A. Sutherland, T. Rabie, A. M. Buchan, Laser Doppler Flowmetry to Measure Changes in Cerebral Blood Flow, Springer New York, New York, NY, 2014, pp. 237–248.

[11] U. Dirnagl, B. Kaplan, M. Jacewicz, W. Pulsinelli, Continuous measurement of cerebral cortical blood flow by laser-Doppler flowmetry in a rat stroke model, J. Cereb. Blood Flow Metab. 9 (5) (1989) 589–596.

[12] S. Mauritzon, F. Ginstman, J. Hillman, K. Wrdell, Analysis of laser doppler flowmetry long-term recordings for investigation of cerebral microcirculation during neurointensive care, Front. Neurol. 16 (2022).

[13] M. Leutenegger, E. Martin-Williams, P. Harbi, T. Thacher, W. Raffoul, M. André, A. Lopez, P. Lasser, T. Lasser, Real-time full field laser doppler imaging, Biomed. Opt. Express 2 (6) (2011) 1470–1477.

[14] M. Atlan, B. C. Forget, C. Boccara, T. Vitalis, A. Rancillac, A. K. Dunn, M. Gross, Cortical blood flow assessment with frequency-domain laser Doppler microscopy, J. Biomed. Opt. 12 (2) (2007) 024019.

[15] D. Wajima, M. Nakamura, K. Horiuchi, H. Miyake, Y. Takeshima, K. Tamura, Y. Motoyama, N. Konishi, H. Nakase, Enhanced cerebral ischemic lesions after two-vein occlusion in diabetic rats, Brain Res. 1309 (2010) 126–135.

[16] D. A. Boas, A. K. Dunn, Laser speckle contrast imaging in biomedical optics, J. Biomed. Opt. 15 (1) (2010) 011109.

[17] E. Potapova, E. Seryogina, V. Dremin, D. Stavtsev, I. Kozlov, E. Zherebtsov, A. Mamoshin, Y. Ivanov, A. Dunaev, Laser speckle contrast imaging of blood microcirculation in pancreatic tissues during laparoscopic interventions, Quantum Electron. 50 (1) (2020) 33.

[18] V. Dremin, E. Potapova, A. Mamoshin, A. Dunaev, E. Rafailov, Monitoring oxidative metabolism while modeling pancreatic ischemia in mice using a multimodal spectroscopy technique, Laser Phys. Lett. 17 (11) (2020) 115605.

[19] V. Kalchenko, Y. Kuznetsov, A. Harmelin, I. V. Meglinski, Label free in vivo laser speckle imaging of blood and lymph vessels, J. Biomed. Opt. 17 (5) (2012) 050502.

[20] E. Zharkikh, V. Dremin, E. Zherebtsov, A. Dunaev, I. Meglinski, Biophotonics methods for functional monitoring of complications of diabetes mellitus, J. Biophotonics 13 (10) (2020) e202000203.

[21] A. K. Dunn, Laser speckle contrast imaging of cerebral blood flow, Ann. Biomed. Eng. 40 (2012) 367–377.

[22] Y. Takeshima, H. Miyake, I. Nakagawa, Y. Motoyama, Y.-S. Park, H. Nakase, Visualization of regional cerebral blood flow dynamics during cortical venous occlusion using laser speckle contrast imaging in a rat model, J. Stroke Cerebrovasc. Dis. 24 (2015) 2200–2206.

[23] S. Tao, T. Zhang, K. Zhou, X. Liu, Y. Feng, W. Zhao, J. Chen, Intraoperative monitoring cerebral blood flow during the treatment of brain arteriovenous malformations in hybrid operating room by laser speckle contrast imaging, Front. Surg. 9 (2022) 855397.

[24] G. Piavchenko, I. Kozlov, V. Dremin, D. Stavtsev, E. Seryogina, K. Kandurova, V. Shupletsov, K. Lapin, A. Alekseyev, S. Kuznetsov, A. Bykov, A. Dunaev, I. Meglinski, Impairments of cerebral blood flow microcirculation in rats brought on by cardiac cessation and respiratory arrest, J. Biophotonics 14 (12) (2021) e202100216.

[25] A. Mangraviti, F. Volpin, J. Cha, S. I. Cunningham, K. Raje, M. J. Brooke, H. Brem, A. Olivi, J. Huang, B. M. Tyler, A. Rege, Intraoperative laser speckle contrast imaging for real-time visualization of cerebral blood flow in cerebrovascular surgery:results from pre-clinical studies, Sci. Rep. 10 (2020) 7614.

[26] C. Wang, L. Xian, X. Chen, Z. Li, Y. Fang, W. Xu, L. Wei, W. Chen, S. Wang, Visualization of cortical cerebral blood flow dynamics during craniotomy in acute subdural hematoma using laser speckle imaging in a rat model, Brain Res. 1742 (2020) 146901.

[27] V. Kalchenko, A. Sdobnov, I. Meglinski, Y. Kuznetsov, G. Molodij, A. Harmelin, A robust method for adjustment of laser speckle contrast imaging during transcranial mouse brain visualization, Photonics 6 (3) (2019) 80.

[28] S. Bricq, G. Mah, D. Rousseau, A. Humeau-Heurtier, F. Chapeau-Blondeau, J. R. Varela, P. Abraham, Assessing spatial resolution versus sensitivity from laser speckle contrast imaging: application to frequency analysis, Med. Biol. Eng. Comput. 50 (2012) 1017–1023.

[29] C. G. Scully, N. Mitrou, B. Braam, W. A. Cupples, K. H. Chon, Detecting physiological systems with laser speckle perfusion imaging of the

renal cortex, Am. J. Physiol. Regul. Integr. Comp. Physiol. 304 (11) (2013) R929–R939.

[30] D. D. Postnov, O. Sosnovtseva, V. V. Tuchin, Improved detectability of microcirculatory dynamics by laser speckle flowmetry, J. Biophotonics 8 (10) (2015) 790–794.

[31] A. Y. Neganova, D. D. Postnov, O. Sosnovtseva, J. C. B. Jacobsen, Rat retinal vasomotion assessed by laser speckle imaging, PLOS ONE 12 (3) (2017) e0173805.

[32] I. Mizeva, V. Dremin, E. Potapova, E. Zherebtsov, I. Kozlov, A. Dunaev, Wavelet analysis of the temporal dynamics of the laser speckle contrast in human skin, IEEE. Trans. Biomed. Eng. 67 (7) (2020) 1882–1889.

[33] I. Mizeva, E. Potapova, V. Dremin, I. Kozlov, A. Dunaev, Spatial heterogeneity of cutaneous blood flow respiratory-related oscillations quantified via laser speckle contrast imaging, PLOS ONE 16 (5) (2021) e0252296.

[34] M. Hultman, M. Larsson, T. Strmberg, J. Henricson, F. Iredahl, I. Fredriksson, Flowmotion imaging analysis of spatiotemporal variations in skin microcirculatory perfusion, Microvasc. Res. 146 (2023) 104456.

[35] K. Basak, M. Manjunatha, P. K. Dutta, Review of laser speckle-based analysis in medical imaging, Med. Biol. Eng. Comput. 50 (2012) 547–558.

[36] M. Draijer, E. Hondebrink, T. van Leeuwen, W. Steenbergen, Review of laser speckle contrast techniques for visualizing tissue perfusion, Lasers Med. Sci. 24 (2009) 639–651.

[37] D. Briers, D. D. Duncan, E. R. Hirst, S. J. Kirkpatrick, M. Larsson, W. Steenbergen, T. Stromberg, O. B. Thompson, Laser speckle contrast imaging: theoretical and practical limitations, J. Biomed. Opt. 18 (6) (2013) 066018.

[38] P. G. Vaz, A. Humeau-Heurtier, E. Figueiras, C. Correia, J. Cardoso, Laser speckle imaging to monitor microvascular blood flow: A review, IEEE Rev. Biomed. Eng. 9 (2016) 106–120.

[39] H. Cheng, T. Q. Duong, Simplified laser-speckle-imaging analysis method and its application to retinal blood flow imaging, Opt. Lett. 32 (15) (2007) 2188–2190.

[40] Y. Li, S. Zhu, L. Yuan, H. Lu, H. Li, S. Tong, Predicting the ischemic infarct volume at the first minute after occlusion in rodent stroke model by laser speckle imaging of cerebral blood flow, J. Biomed. Opt. 18 (7) (2013) 076024.

[41] M. Brai, A. Stefanovska, Wavelet-based analysis of human blood-flow dynamics, Bulletin of Mathematical Biology 60 (1998) 919–935.

[42] P. Goupillaud, A. Grossmann, J. Morlet, Cycle-octave and related transforms in seismic signal analysis, Geoexploration 23 (1) (1984) 85–102.

[43] Z. Li, E. W. C. Tam, M. P. C. Kwan, A. F. T. Mak, S. C. L. Lo, M. C. P. Leung, Effects of prolonged surface pressure on the skin blood flowmotions in anaesthetized rats – an assessment by spectral analysis of laser doppler flowmetry signals, Phys. Med. Biol. 51 (10) (2006) 2681.

[44] V. V. Aleksandrin, A. V. Ivanov, E. D. Virus, P. O. Bulgakova, A. A. Kubatiev, Application of wavelet analysis to detect dysfunction in cerebral blood flow autoregulation during experimental hyperhomocysteinaemia, Lasers Med. Sci. 33 (2018) 1327–1333.

[45] N. Bosschaart, G. J. Edelman, M. C. G. Aalders, T. G. van Leeuwen, D. J. Faber, A literature review and novel theoretical approach on the optical properties of whole blood, Lasers Med. Sci. 29 (2014) 453–479.

[46] B. Aernouts, R. V. Beers, R. Watté, J. Lammertyn, W. Saeys, Dependent scattering in Intralipid® phantoms in the 600-1850 nm range, Opt. Express 22 (5) (2014) 6086–6098.

[47] H. Soleimanzad, F. Smekens, J. Peyronnet, M. Juchaux, O. Lefebvre, D. Bouville, C. Magnan, H. Gurden, F. Pain, Multiple speckle exposure imaging for the study of blood flow changes induced by functional activation of barrel cortex and olfactory bulb in mice, Neurophotonics 6 (1) (2019) 015008.

[48] M. Z. Ansari, E.-J. Kang, M. D. Manole, J. P. Dreier, A. Humeau-Heurtier, Monitoring microvascular perfusion variations with laser

speckle contrast imaging using a view-based temporal template method, Microvasc. Res. 111 (2017) 49–59.

[49] V. Kalchenko, D. Israeli, Y. Kuznetsov, I. Meglinski, A. Harmelin, A simple approach for non-invasive transcranial optical vascular imaging (nTOVI), J. Biophotonics 8 (11-12) (2015) 897–901.

[50] J. O'Doherty, P. McNamara, N. T. Clancy, J. G. Enfield, M. J. Leahy, Comparison of instruments for investigation of microcirculatory blood flow and red blood cell concentration, J. Biomed. Opt. 14 (3) (2009) 034025.

[51] K. Ivanov, M. Kalinina, Y. Levkovich, Blood flow velocity in capillaries of brain and muscles and its physiological significance, Microvasc. Res. 22 (2) (1981) 143–155.

[52] T. Mastantuono, N. Starita, L. Battiloro, M. Di Maro, M. Chiurazzi, G. Nasti, E. Muscariello, M. Cesarelli, L. Iuppariello, G. DAddio, A. Gorbach, A. Colantuoni, D. Lapi, Laser speckle imaging of rat pial microvasculature during hypoperfusion-reperfusion damage, Front. Cell. Neurosci. 11 (2017) 298.

[53] P. Vaz, T. Pereira, E. Figueiras, C. Correia, A. Humeau-Heurtier, J. Cardoso, Which wavelength is the best for arterial pulse waveform extraction using laser speckle imaging?, Biomed. Signal Process. Control 25 (2016) 188–195.

[54] M. J. Davis, Myogenic response gradient in an arteriolar network, Am. J. Physiol. Heart Circ. 264 (6) (1993) H2168–H2179.

[55] J. R. Whittaker, I. D. Driver, M. Venzi, M. G. Bright, K. Murphy, Cerebral autoregulation evidenced by synchronized low frequency oscillations in blood pressure and resting-state fmri, Front. Neurosci. 13 (2019) 433.

[56] D. Zhu, K. V. Larin, Q. Luo, V. V. Tuchin, Recent progress in tissue optical clearing, Laser Photonics Rev. 7 (5) (2013) 732–757.

[57] E. Kornaeva, I. Stebakov, A. Kornaev, V. Dremin, S. Popov, A. Vinokurov, A method to measure non-Newtonian fluids viscosity using inertial viscometer with a computer vision system, Int. J. Mech. Sci. 242 (2023) 107967.